Bound and resonance states of the dipolar anion of hydrogen cyanide: Competition between threshold effects and rotation in an open quantum system

K. Fossez,[1] N. Michel,[1] W. Nazarewicz,[2,3,4] M. Płoszajczak,[1] and Y. Jaganathen[5,6]

[1]*Grand Accélérateur National d'Ions Lourds (GANIL), CEA/DSM - CNRS/IN2P3, BP 55027, F-14076, Caen, France*

[2]*Department of Physics and Astronomy and NSCL/FRIB Laboratory, Michigan State University, East Lansing, Michigan 48824, USA*

[3]*Physics Division, Oak Ridge National Laboratory, P. O. Box 2008, Oak Ridge, Tennessee 37831, USA*

[4]*Institute of Theoretical Physics, Faculty of Physics, University of Warsaw, Warsaw, Poland*

[5]*Department of Physics & Astronomy, University of Tennessee, Knoxville, Tennessee 37996, USA*

[6]*NSCL/FRIB Laboratory, Michigan State University, East Lansing, Michigan 48824, USA*

(Received 24 October 2014; published 12 January 2015)

Bound and resonance states of the dipole-bound anion of hydrogen cyanide HCN^- are studied using a nonadiabatic pseudopotential method and the Berggren expansion technique involving bound states, decaying resonant states, and nonresonant scattering continuum. We devise an algorithm to identify the resonant states in the complex energy plane. To characterize spatial distributions of electronic wave functions, we introduce the body-fixed density and use it to assign families of resonant states into collective rotational bands. We find that the nonadiabatic coupling of electronic motion to molecular rotation results in a transition from the strong-coupling to weak-coupling regime. In the strong-coupling limit, the electron moving in a subthreshold, spatially extended halo state follows the rotational motion of the molecule. Above the ionization threshold, the electron's motion in a resonance state becomes largely decoupled from molecular rotation. The widths of resonance-band members depend primarily on the electron orbital angular momentum.

DOI: 10.1103/PhysRevA.91.012503 PACS number(s): 31.15.V−, 03.65.Nk, 33.15.Ry

I. INTRODUCTION

Dipolar anions are one of the most spectacular examples of marginally bound quantum systems [1–11]. Wave functions of electrons coupled to neutral dipole molecules [12,13] are extremely extended; they form the extreme quantum halo states [14–19]. Resonance energies of dipolar anions, including those associated with rotational threshold states, can been determined in high-resolution electron photodetachment experiments [20–25]. Theoretically, however, the literature on the unbound part of the spectrum of dipole potentials, and multipolar anions in particular, is fairly limited [26–34].

The breakdown of the adiabatic approximation in dipolar molecules possessing a supercritical moment [35–39] caused by the coupling of an electron's motion to the rotational motion of the molecule, is expected to profoundly impact the properties of rotational bands in such systems [25,30,31,36], such as the the number of rotationally excited bound anion states.

In this study, we address the nature of the unbound part of the spectrum of dipolar anions. In particular, we are interested in elucidating the transition from the rotational motion of weakly bound subthreshold states to the rotational-like behavior exhibited by unbound resonances. The competition between continuum effects, collective rotation, and nonadiabatic aspects of the problem makes the description of threshold states in dipole-bound molecules both interesting and challenging.

Our theoretical framework is based on the Berggren expansion method (BEM), a complex-energy resonant-state expansion [40–42] based on a completeness relation introduced by Berggren [43] that involves bound, decaying, and scattering states. In the context of the coupled-channel method, BEM was successfully applied to molecules [39] and nuclei [44–49]. The advantage of this method, which is of particular importance to the problem of dipole-bound anions when the rotational motion of the molecule is considered [39,50], is that the BEM is largely independent of the precise implementation of boundary conditions at infinity.

This is not the case for other techniques such as, for instance, the direct method of integrating coupled-channel equations. Notable exceptions are basis-expansion methods relying on complex scaling [51–57]. By rotating radial coordinates in the complex plane by an given angle θ,$r \rightarrow re^{i\theta}$, the initial Hermitian Hamiltonian is transformed into a non-Hermitian one, whose bound eigenstates correspond to bound and resonant states of the system, the second of these bearing complex energies. As complex-scaled wave functions all vanish for $r \rightarrow +\infty$, their asymptotic behavior does not have to be imposed explicitly and they can be obtained through a diagonalization of the rotated Hamiltonian in a set of square-integrable states [55,57–60]. In particular, BEM has been benchmarked against complex rotation when both methods apply [59,60]. However, rotation by an angle θ of the Hamiltonian is possible only if the potential is dilatation-analytic [61,62]. This is obviously the case for the exact molecular Hamiltonian, but not necessarily the case for effective pseudopotentials. In fact, pseudopotentials can be nonanalytical or diverge in the complex plane for small values of θ, as is the case for the pseudopotential studied in this paper. Complex rotation of the Hamiltonian is thus precluded. The BEM, on the other hand, can be conveniently applied. An alternative treatment, similar in spirit, is the complex eigenvalue Schrödinger equation (CESE) method [63,64].

The calculations have been carried out for the rotational spectrum of dipole-bound anions of hydrogen cyanide HCN^-, which has long served as a prototype of a dipole-bound anion [4,65] and was a subject of experimental and theoretical studies [25,66,67]. Here, we extend our previous studies [39] of bound states of dipolar molecules to the unbound part of the

spectrum. To integrate coupled-channel equations, we use the Berggren expansion method as it offers superior accuracy as compared to the direct integration approach for weakly bound states and, contrary to the direct integration approach, allows to describe unbound resonant states. Moreover, the knowledge of the asymptotic form of eigenfunctions is not necessary in our approach.

This paper is organized as follows. The model Hamiltonian is discussed in Sec. II. The coupled-channel formulation of the Schrödinger equation for dipole-bound anions is outlined in Sec. III. The Berggren expansion method is introduced in Sec. IV. The parameters of our calculation are given in Sec. V. Section VI presents the technique adopted to identify the decaying Gamow states (resonances). To visualize the valence electron distributions, in Sec. VII we introduce the intrinsic one-body density. The predictions for bound states and resonances of HCN^- are collected in Sec. VIII. Finally, Sec. IX contains the conclusions and outlook.

II. HAMILTONIAN

The dipolar anions are composed of a neutral polar molecule with a dipole moment μ that is large enough to bind an additional electron. Since the energy of the valence electron in an anion is very small as compared to the energies of well-bound HCN electrons, this scale separation justifies the use of an effective potential treatment of the halo [68–70]. In the present study, the HCN^- dipolar anion is described in the Born-Oppenheimer approximation, and the intrinsic spin of an external electron is neglected [35], largely simplifying the equations [36]. Within the pseudopotential method, the Hamiltonian of a dipolar anion can be written as

$$H = \frac{\boldsymbol{p}_e^2}{2m_e} + \frac{\boldsymbol{j}^2}{2I} + V, \tag{1}$$

where I is the moment of inertia of the molecule, $\boldsymbol{p}_e$ is the linear momentum of the valence electron, and m_e its mass. The electron-molecule interaction V is approximated by a one-body pseudopotential [35,71,72]

$$V(r,\theta) = V_{\rm dip}(r,\theta) + V_\alpha(r,\theta) + V_{Q_{zz}}(r,\theta) + V_{\rm SR}(r), \tag{2}$$

where θ is the angle between the dipolar charge separation $\boldsymbol{s}$ and electron coordinate;

$$V_{\rm dip}(r,\theta) = -\mu e \sum_{\lambda=1,3,\ldots,} \left(\frac{r_<}{r_>}\right)^\lambda \frac{1}{sr_>} P_\lambda(\cos\theta) \tag{3}$$

is the electric dipole potential of the molecule;

$$V_\alpha(r,\theta) = -\frac{e^2}{2r^4}[\alpha_0 + \alpha_2 P_2(\cos\theta)] f(r) \tag{4}$$

is the induced dipole potential, where α_0 and α_2 are the spherical and quadrupole polarizabilities of the linear molecule;

$$V_{Q_{zz}}(r,\theta) = -\frac{e}{r^3} Q_{zz} P_2(\cos\theta) f(r) \tag{5}$$

is the potential due to the permanent quadrupole moment of the molecule; and

$$V_{\rm SR}(r) = V_0 \exp[-(r/r_c)^6] \tag{6}$$

is the short-range potential, where r_c is a radius range. The short-range potential accounts for the exchange effects and compensates for spurious effects induced by the regularization function

$$f(r) = 1 - \exp[-(r/r_0)^6] \tag{7}$$

introduced in Eqs. (4) and (5) to avoid a singularity at $r \to 0$. The parameter r_0 in Eq. (7) defines an effective short range for the regularization.

The dipolar potential $V_{\rm dip}(r,\theta)$ is discontinuous at $r = s$. To remove this discontinuity, in Eq. (3) we replace

$$\frac{r_>}{r_<} \longrightarrow \left\{\frac{r}{s} f_a(r) + \frac{s}{r}[1 - f_a(r)]\right\} \mathrm{erf}(ar), \tag{8}$$

$$r_> \longrightarrow s f_a(r) + r[1 - f_a(r)], \tag{9}$$

with $f_a(r) = (1 + \exp[(r-s)/a])^{-1}$.

III. COUPLED-CHANNEL EQUATIONS

In the description of dipolar anions with the Hamiltonian (1), the coupled-channel formalism is well adapted to express the wave function of the system [1, 35,72–74]. The eigenfunction of H corresponding to the total angular momentum J can be written as

$$\Psi^J = \sum_c u_c^J(r) \Theta^J_{\ell_c j_c}, \tag{10}$$

where the index c labels the channel (ℓ, j), $u_c^J(r)$ is the radial wave function of the valence electron, $\Theta^J_{\ell_c j_c}$ is the channel function, and $\boldsymbol{j} + \boldsymbol{\ell} = \boldsymbol{J}$. Since the Hamiltonian is rotationally invariant, its eigenvalues are independent of the magnetic quantum number M_J, which will be omitted in the following.

To write the Schrödinger equation as a set of coupled-channel equations, the potential $V(r,\theta)$ in Eqs. (2) to (6) is expanded in multipoles

$$V(r,\theta) = \sum_\lambda V_\lambda(r) P_\lambda(\cos\theta), \tag{11}$$

where $V_\lambda(r)$ is the radial form factor and

$$P_\lambda(\cos\theta) = \frac{4\pi}{2\lambda+1} Y_\lambda^{(\rm mol)}(\hat{\boldsymbol{s}}) \cdot Y_\lambda^{(e)}(\hat{\boldsymbol{r}}). \tag{12}$$

The matrix elements $\langle \Theta^J_{\ell_{c'} j_{c'}} | P_\lambda(\cos\theta) | \Theta^J_{\ell_c j_c} \rangle$ are obtained by means of the standard angular momentum algebra [39]. The resulting coupled-channel equations for the radial wave functions $u_c^J(r)$ can be written as

$$\left[\frac{d^2}{dr^2} - \frac{\ell_c(\ell_c+1)}{r^2} - \frac{j_c(j_c+1)}{I} + E_J\right] u_c^J(r) = \sum_{c'} V^J_{cc'}(r) u^J_{c'}(r), \tag{13}$$

where E_J is the energy of the system and

$$V^J_{cc'}(r) = \sum_\lambda \left\langle \Theta^J_{\ell_{c'} j_{c'}} \middle| P_\lambda(\cos\theta) \middle| \Theta^J_{\ell_c j_c} \right\rangle V_\lambda(r) \tag{14}$$

is the coupling potential. Due to an r^6 dependence of exponents in Eqs. (6) and (7), the resulting pseudopotential is non-dilatation-analytic.

IV. BERGGREN EXPANSION METHOD

The Berggren expansion method for studies of the bound states of dipolar anions has been introduced in Ref. [39]. In this method, the Hamiltonian is diagonalized in a complete basis of single-particle (s.p.) states, the so-called Berggren ensemble [41–43], which is generated by a finite-depth spherical one-body potential. The Berggren ensemble contains bound (b), decaying (d), and scattering (s) single-particle states along the contour $\mathcal{L}^+_{\ell,j}$ for each considered partial wave (ℓ, j). For that reason, the Berggren ensemble is ideally suited to deal with weakly bound and unbound structures having large spatial extensions, such as halos, Rydberg states, or decaying resonances. For more details and recent applications of BEM in the many-body context see Ref. [75] and references cited therein.

While the finite-depth potential generating the Berggren ensemble can be chosen arbitrarily, to improve the convergence we take the diagonal part of the channel coupling potential $V_{cc'}(r)$. Indeed, since all basis states of a channel c have the same values of ℓ_c and j_c, changing their generating potential only amounts to applying a unitary transformation. Hence, the most optimal potential is that for which all couplings between states of a given channel c vanish, which is the case for $V_{cc}(r)$. The basis states $\Phi_{k,c}(r)$ are eigenstates of the spherical potential $V_{cc}(r)$, which are regular at origin and meet outgoing (b,d) and scattering (s) boundary conditions. Note that the wave number k characterizing eigenstates $\Phi_{k,c}(r)$ is in general complex. The normalization of the bound states is standard, while that for the decaying states involves the exterior complex scaling [39,75–78]. The scattering states are normalized to the Dirac delta function.

To determine the Berggren ensemble, one calculates first the s.p. bound and resonance states of the generating s.p. potential for all chosen partial waves (ℓ, j). Then, for each channel (ℓ, j), one selects the contour $\mathcal{L}^+_{\ell,j}$ in a fourth quadrant of the complex k plane. All (ℓ, j) scattering states in this ensemble belong to $\mathcal{L}^+_{\ell,j}$. The precise form of $\mathcal{L}^+_{\ell,j}$ is unimportant providing that all selected s.p. resonances for a given (ℓ, j) lie between this contour and the real k axis for $\mathrm{Re}(k) > 0$. For each channel, the set of all resonant states and scattering states on $\mathcal{L}^+_{\ell_c,j_c}$ forms a complete s.p. basis.

In the present study, each contour $\mathcal{L}^+_{\ell,j}$ is composed of three segments: the first one from the origin to k_{peak} in the fourth quadrant of the complex k plane, the second one from k_{peak} to k_{middle} on the real k axis ($\mathrm{Re}(k) > 0$), and the third one from k_{middle} to k_{max} also on the real k axis. In all practical applications of the BEM, each contour $\mathcal{L}^+_{\ell j}$ is discretized and the Gauss-Legendre quadrature is applied. The cutoff momentum $k = k_{\mathrm{max}}$ should be sufficiently large to guarantee the completeness to a desired precision. The discretized scattering states $|\Phi_{n,c}\rangle$ are renormalized using the Gauss-Legendre weights. In this way, the Dirac delta normalization of the scattering states is replaced by the usual Kronecker delta normalization. In this way, all $|\Phi_{i,c}\rangle$ states can be treated on the same footing in the discretized Berggren completeness relation

$$\sum_{i=1}^{N} |\Phi_{i,c}\rangle \langle\Phi_{i,c}| \simeq 1, \tag{15}$$

where the N basis states include bound, resonance, and discretized scattering states for each considered channel c.

The Hamiltonian matrix can be computed straightforwardly in the discretized Berggren basis [39]. The diagonal matrix elements are

$$\langle\Phi_{i,c}|H|\Phi_{i,c}\rangle = \left(k_i^2 + \frac{j_c(j_c+1)}{I}\right). \tag{16}$$

To compute off-diagonal matrix elements, we apply the exterior complex scaling [53,76,78,79]

$$\begin{aligned}\langle\Phi_{i',c'}|H|\Phi_{i,c}\rangle &= \langle\Phi_{i',c'}|V|\Phi_{i,c}\rangle \\ &= \int_0^R \Phi_{i',c'}(r) V_{cc'}(r)\, \Phi_{i,c}(r)\, dr \\ &\quad + \sum_{ss'=\pm} \int_0^{+\infty} \Phi^{(s')}_{i',c'}[z(x)] V_{cc'}(z(x)) \\ &\quad \times \Phi^{(s)}_{i,c}[z(x)]\, e^{i\theta}\, dx, \end{aligned} \tag{17}$$

where $z(x) = R + xe^{i\theta}$, $\Phi^{(\pm)}_{i,c}(r)$ is the outgoing or incoming part of $\Phi_{i,c}(r)$, θ is a complex rotation angle chosen according to the asymptotic behavior of $\Phi^{(\pm)}_{i,c}(r)$. The radius R is chosen sufficiently large so that the exponentials of Eqs. (6) and (7) can be suppressed in the real asymptotic region. Since the coupling potential $V_{cc'}(r)$ in Eq. (17) decreases at least as fast as r^{-2} in the complex plane, no singularities occur. Due to the completeness of the Berggren ensemble, the representation of the Hamiltonian by the matrix (16) and (17) is exact, up to contour discretization and momentum truncation.

V. PARAMETERS OF THE BEM CALCULATION

The parameters of the pseudopotential for the HCN^- anion are taken from Ref. [36]. These are

$$\begin{aligned} \alpha_0 &= 15.27\, a_0^3, \\ \alpha_2 &= 1.08\, a_0^3, \\ Q_{zz} &= 3.28\, e a_0^2, \\ I &= 7.42 \times 10^4\, m_e a_0^2, \\ r_0 &= 4.4\, a_0, \\ r_c &= 3.071622666\, a_0, \\ V_0 &= 4.0\, \mathrm{Ry}, \\ s &= 2.04\, a_0, \end{aligned}$$

and $a = a_0$. The value of r_c has been adjusted to reproduce the experimental ground-state ($J^\pi = 0^+$) energy [25]: $E^{\mathrm{exp}}(0^+_1) = -1.1465789 \times 10^{-4}$ Ry. For the dipolar moment of the molecule, we take the experimental value $\mu = 1.174\, ea_0$. In the following, we express r in units of the Bohr radius a_0, I in units of $m_e a_0^2$, and energy in Ry. The $J^\pi = 1^-$ band-head energy is also known experimentally, $E^{\mathrm{exp}}(1^-_1) = -8.8198377 \times 10^{-5}$ Ry, but no adjustment of the model parameters has been attempted to fit the experimental value.

To achieve stability of bound-state energies, the BEM calculations were carried out by including all partial waves with $\ell \leqslant \ell_{\mathrm{max}} = 9$ and taking the optimized number of points ($N_{\mathrm{C}} = 165$) on the complex contour with $k_{\mathrm{max}} = 6\, a_0^{-1}$ for

each J^π. For all (ℓ, j) channels and all J^π values, the complex contour $\mathcal{L}^+_{\ell,j}$ is taken close to the real axis ($k_{\rm peak} = 0.15 - i10^{-7}$,$k_{\rm middle} = 1.0$, and $k_{\rm max} = 6.0$; all in a_0^{-1}). Its precise form has been adjusted by looking at the convergence of bound-state energies when changing the imaginary part of $k_{\rm peak}$. Each segment of any contour $\mathcal{L}^+_{\ell,j}$ is discretized with the same number of points ($N_{\rm C}/3 = 55$).

VI. IDENTIFICATION OF THE RESONANCES

The diagonalization of a complex-symmetric Hamiltonian matrix in BEM yields a set of eigenenergies which are the physical states (poles of the resolvent of the Hamiltonian) and a large number of complex-energy scattering states. The resonances are thus embedded in a discretized continuum of scattering states and their identification is not trivial [80,81].

The eigenstates associated with resonances should be stable with respect to changes of the contour [80,81]. Moreover, their dominant channel wave functions should exhaust a large fraction of the real part of the norm. The norm of an eigenstate of the Hamiltonian is given by

$$\sum_c \sum_i \langle \Phi_{k,c} | u_c \rangle^2 = \sum_c n_c = 1, \tag{18}$$

where n_c the norm of the channel wave function. In general, the norms of individual channel wave functions for resonances are complex numbers and their real parts are not necessarily positive-definite. It may happen that if a large number of weak channels $\{c_i\}$ with small negative norms ${\rm Re}(n_{c_i}) < 0$ contribute to the resonance wave function, then the dominant channel c can have a norm $n_c > 1$. This does not come as a surprise as the channel wave functions have no obvious probabilistic interpretation.

To check the stability of BEM eigenstates, we varied the imaginary part of $k_{\rm peak}$ from 0 to $-0.0001 a_0^{-1}$ in all partial-wave contours. Resulting contour variations change both the real $\Delta{\rm Re}(E) \ll {\rm Re}(E)$ and imaginary $\Delta{\rm Im}(E)$ parts of the eigenenergies. The precision of the resonance-identification method is assessed by looking at the ratio $\Delta{\rm Im}(E)/{\rm Im}(E)$, which is in the range [0.001,0.3] for the resonance states. As an example, the eigenvalues of $J^\pi = 2^+$ resonant states are listed in Table I. It is seen that the relative variations of ${\rm Re}(E)$ are always smaller than 1%, while the relative variations of ${\rm Im}(E)$ can reach ∼15%. Moreover, values of $\Delta{\rm Im}(E)/{\rm Im}(E)$ for different resonant states can differ by three orders of magnitude. In general, a better stability of the BEM eigenstates and, i.e., smaller values of $\Delta{\rm Im}(E)/{\rm Im}(E)$, are found for those eigenstates, which have several channel wave functions contributing significantly to the total norm. A typical accumulation of eigenenergies when changing the contour is shown in Fig. 1. One can see that the nonresonant states do not exhibit the degree of stability that is typical of resonant states. It is interesting to notice that several resonant states are found fairly away from the region of nonresonant eigenstates. The stability of resonant eigenstates persists if the real part of $k_{\rm peak}$ is varied from 0.14 a_0^{-1} to 0.16 a_0^{-1}. In this case, the relative variations of the real part of the eigenstate energies dominate as can be seen in Fig. 2 for the two near-threshold resonances labeled 2 and 3 in Table I.

TABLE I. Relative variation of the real part $\delta{\rm Re}(E) = \Delta{\rm Re}(E)/{\rm Re}(E)$ (in percent) and imaginary part $\delta{\rm Im}(E) = \Delta{\rm Im}(E)/{\rm Im}(E)$ (in percent) of energies of twenty $J^\pi = 2^+$ resonances with the change of $k_{\rm peak}$. All energies are in Ry. The numbers in parentheses denote powers of 10.

resonance	Re(E)	δRe(E)	Im(E)	δIm(E)
1	2.51(−5)	2.47(−1)	−9.68(−6)	2.09(−1)
2	2.69(−4)	1.29(−4)	−3.45(−10)	1.32(+1)
3	2.77(−4)	1.37(−5)	−3.58(−9)	1.56(+1)
4	3.55(−4)	5.61(−4)	−7.20(−7)	1.60
5	3.67(−4)	3.70(−4)	−1.21(−6)	1.78
6	3.96(−4)	3.52(−3)	−2.34(−6)	4.55(−1)
7	3.98(−4)	2.07(−2)	−5.05(−5)	6.19(−2)
8	4.25(−4)	6.02(−3)	−1.04(−4)	3.02(−2)
9	6.48(−4)	9.70(−5)	−6.72(−7)	1.42
10	6.60(−4)	6.86(−4)	−8.32(−7)	2.52
11	6.81(−4)	6.77(−3)	−1.19(−5)	7.41(−1)
12	6.86(−4)	9.86(−4)	−1.60(−6)	1.55
13	7.40(−4)	5.05(−3)	−6.68(−5)	3.85(−2)
14	9.80(−4)	7.89(−4)	−7.86(−7)	1.45(+1)
15	1.05(−3)	4.80(−5)	−6.22(−7)	1.39
16	1.06(−3)	1.87(−4)	−8.54(−7)	2.66
17	1.07(−3)	1.82(−3)	−5.60(−6)	1.10
18	1.09(−3)	4.00(−4)	−4.89(−7)	7.67
19	1.11(−3)	8.05(−4)	−1.66(−6)	9.61
20	1.14(−3)	2.28(−3)	−2.71(−5)	1.31(−1)

To demonstrate that the identified resonances are stable with respect to $\ell_{\rm max}$, in Fig. 3 we show the energy convergence for states 1 to 3 of Table I. In general, Im(E) is significantly more sensitive than Re(E) with respect to the addition of channels with higher ℓ and j values. It is seen that Im(E) for resonances with the dominant channels ($\ell = 4, j = 4$) and ($\ell = 3, j = 1$)

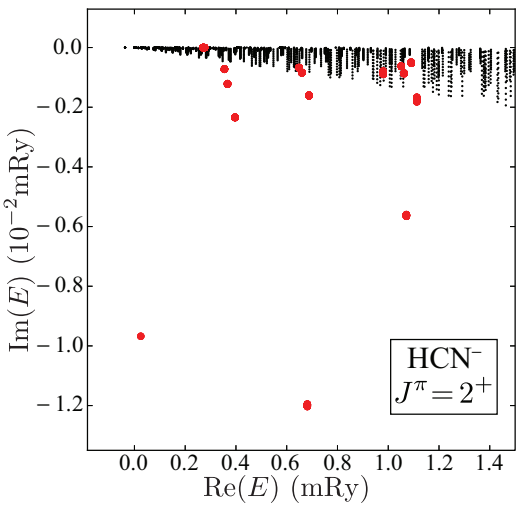

FIG. 1. (Color online) Illustration of the stability of the energies of the $J^\pi = 2^+$ resonant states of HCN^- listed in Table I (large dots) when the nonresonant scattering contour is shifted. Here, the imaginary part of $k_{\rm peak}$ was varied from 0 to $-0.0001 a_0^{-1}$. As a comparison, nonresonant eigenenergies are marked with tiny dots and exhibit significant shifts.

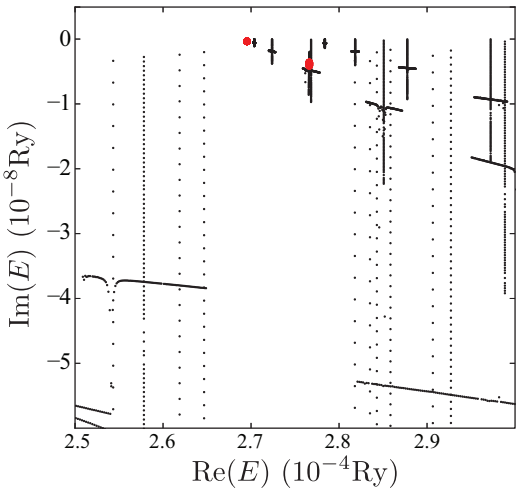

FIG. 2. (Color online) Similar as in Fig. 1 but zoomed in on the two threshold resonances (states 2 and 3 in Table I). Here, the real part of $k_{\rm peak}$ is also varied from 0.14 a_0^{-1} to 0.16 a_0^{-1}.

are converged already for $\ell_{\rm max} \geqslant 6$. The convergence for the narrow resonance with the dominant channel $(\ell = 2, j = 4)$ shown in Fig. 3(a) is also excellent, considering that in this case Im(E) is of the order of 10^{-10} Ry, which is close to the limit of a numerical precision of our BEM calculations.

VII. INTRINSIC DENSITY

It is instructive to present the density of the valence electron in the body-fixed frame. This can easily be done in the strong coupling scheme of the particle-plus-rotor model [82–84], which is usually formulated in the K representation associated with the intrinsic frame. Here, $K_J = K_\ell + K_j$ is the projection of the total angular momentum on the symmetry axis of the molecule. Of particular interest is the adiabatic limit of $I \to \infty$, where all J^π members of a rotational band collapse at the band head, i.e., they all can be associated with one intrinsic

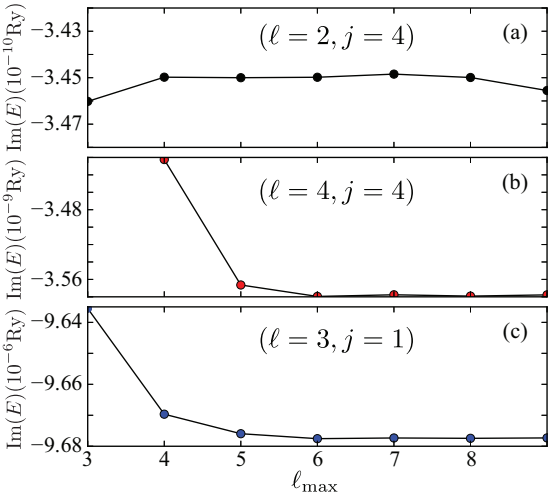

FIG. 3. (Color online) The convergence of Im(E) for $J^\pi = 2^+$ resonances (a) 2, (b) 3, and (c) 1 of Table I as a function of $\ell_{\rm max}$. The quantum numbers (ℓ, j) of the dominant channel are indicated.

configuration. The K representation is useful to visualize wave functions, group states with different J values into rotational bands, and interpret the results in terms of Coriolis mixing [47,50,85–88].

In the body-fixed frame, the density of the valence electron in the state J^π is axially symmetric and can be decomposed as

$$\rho_J(r,\theta) = \sum_{K_J} \rho_{JK_J}(r,\theta), \tag{19}$$

where (r,θ) stand for the polar coordinates of the electron in the intrinsic frame, and the K_J components of the density are

$$\rho_{JK_J}(r,\theta) = \sum_{\ell,\ell'} \sum_j \frac{2j+1}{2J+1} \langle \ell K_J j 0 | J K_J \rangle \langle \ell' K_J j 0 | J K_J \rangle \times \frac{u^J_{\ell j}(r)^*}{r} \frac{u^J_{\ell' j}(r)}{r} Y_\ell^{K_J *}(\theta,0)\, Y_{\ell'}^{K_J}(\theta,0). \tag{20}$$

If all K_J components except one vanish in Eq. (19), the adiabatic strong-coupling limit is reached and K_J becomes a good quantum number. In this particular case, ρ_{JK_J} can be identified as the intrinsic electronic density in the dipole-fixed reference frame. To quantify the degree of K_J mixing, it is convenient to introduce the normalization amplitudes

$$n_{JK_J} = \sum_{\ell,j} \frac{2j+1}{2J+1} \langle \ell K_J j 0 | J K_J \rangle^2 \int \left| u^J_{\ell j}(r) \right|^2 dr. \tag{21}$$

Due to Eq. (18), n_{JK_J} fullfil the normalization condition

$$\sum_{K_J} n_{JK_J} = 1. \tag{22}$$

VIII. RESULTS OF BEM CALCULATIONS

Predicted energy spectra of HCN^- with $J^\pi = 0^+,1^-,2^+,3^-,4^+$, and 5^- are shown in Table II. One may notice that the calculated energy of the 1^- band head $E(1_1^-) = -8.96 \times 10^{-5}$ Ry is close to the experimental value $E^{\rm exp}(1_1^-) = -8.82 \times 10^{-5}$ Ry. Moreover, consistently with earlier Refs. [25,36], we do not find a $J^\pi = 3^-$ bound state.

The states listed in Table II are plotted in Fig. 4 in the complex energy plane. These states can be assembled according to their decay widths into five groups labeled g_0 to g_4. The group 4 contains bound states and very narrow threshold resonances of the dipolar anion. Narrow resonances are contained in groups 3 and 2 while broader states form groups 1 and 0. The characterization of the resonance spectra of HCN^- in terms of groups g_0 to g_4 will be provided below.

A. Adiabatic limit

To check the numerical accuracy of the adiabatic approximation, we computed the energies of the lowest states of HCN^- in the adiabatic limit of $I \to \infty$ (in practice, $I = 10^{16}\, m_e a_0^2$). In this limit, which can be associated with the extreme strong coupling regime, K_J becomes a good quantum number and energies of all band members $J = K_J, K_J + 1, K_J + 2, \ldots,$ collapse at the band head $E_{J=K_J}$. In our calculations, the maximum energy difference between the members of the ground-state band $(J^\pi = 0_1^+,1_1^-,2_1^+,3_1^-,4_1^+,5_1^-)$ is 1.5×10^{-7} Ry, which is better than 0.1% of the energy of the 0^+ state

TABLE II. Predicted complex energies (in Ry) of bound and resonance $0^+,1^-,2^+,3^-,4^+$, and 5^- states of the HCN^- dipolar anion. Numbers in the parentheses denote powers of 10.

State	$E(0^+)$	$E(1^-)$	$E(2^+)$	$E(3^-)$	$E(4^+)$	$E(5^-)$
1	−1.15(−4)	−8.96(−5)	−3.69(−5)	3.89(−8) − *i* 1.06(−8)	2.70(−5) − *i* 5.55(−9)	8.09(−5) − *i* 3.08(−9)
2	7.62(−5) − *i* 3.79(−6)	2.70(−5) − *i* 9.98(−10)	2.51(−5) − *i* 9.68(−6)	2.63(−4) − *i* 1.88(−6)	1.84(−4) − *i* 2.02(−6)	1.33(−4) − *i* 2.02(−6)
3	9.35(−4) − *i* 9.69(−5)	8.12(−5) − *i* 7.04(−7)	2.69(−4) − *i* 3.45(−10)	3.03(−4) − *i* 9.25(−6)	2.25(−4) − *i* 2.47(−5)	1.63(−4) − *i* 3.71(−5)
4	1.09(−3) − *i* 1.24(−5)	1.62(−4) − *i* 4.77(−10)	2.77(−4) − *i* 3.58(−9)	4.99(−4) − *i* 1.28(−6)	3.65(−4) − *i* 1.40(−6)	2.56(−4) − *i* 1.87(−6)
5	1.11(−3) − *i* 4.06(−4)	4.88(−4) − *i* 7.04(−7)	3.55(−4) − *i* 7.20(−7)	5.32(−4) − *i* 1.01(−6)	3.99(−4) − *i* 1.43(−6)	2.91(−4) − *i* 1.85(−6)
6	1.14(−3) − *i* 1.62(−5)	5.00(−4) − *i* 1.02(−6)	3.67(−4) − *i* 1.21(−6)	5.69(−4) − *i* 1.25(−4)	4.23(−4) − *i* 1.26(−4)	3.03(−4) − *i* 1.22(−4)
7	1.16(−3) − *i* 2.19(−4)	5.28(−4) − *i* 1.65(−6)	3.96(−4) − *i* 2.34(−6)	8.20(−4) − *i* 1.17(−5)	6.58(−4) − *i* 9.78(−7)	4.94(−4) − *i* 1.03(−6)
8	1.19(−3) − *i* 1.96(−5)	5.34(−4) − *i* 3.13(−5)	3.98(−4) − *i* 5.05(−5)	8.80(−4) − *i* 2.96(−7)	6.91(−4) − *i* 3.44(−7)	5.28(−4) − *i* 3.62(−7)
9	1.27(−3) − *i* 2.13(−5)	5.71(−4) − *i* 9.11(−5)	4.25(−4) − *i* 1.04(−4)	9.39(−4) − *i* 9.91(−5)	6.92(−4) − *i* 1.07(−5)	5.67(−4) − *i* 9.80(−5)
10	1.31(−3) − *i* 3.45(−4)	6.71(−4) − *i* 3.31(−4)	6.48(−4) − *i* 6.72(−6)	1.07(−3) − *i* 3.55(−4)	7.40(−4) − *i* 1.01(−4)	5.92(−4) − *i* 9.87(−6)
11	1.43(−3) − *i* 5.64(−6)	8.37(−4) − *i* 6.53(−7)	6.60(−4) − *i* 8.32(−7)	1.16(−3) − *i* 1.24(−5)	8.66(−4) − *i* 3.38(−4)	6.82(−4) − *i* 3.14(−4)
12	1.84(−3) − *i* 1.10(−5)	8.48(−4) − *i* 8.03(−7)	6.81(−4) − *i* 1.19(−5)	1.30(−3) − *i* 7.87(−7)	9.75(−4) − *i* 1.15(−5)	8.21(−4) − *i* 1.23(−5)
13	3.35(−3) − *i* 1.42(−4)	8.63(−4) − *i* 8.45(−6)	6.88(−4) − *i* 1.60(−6)	1.34(−3) − *i* 1.09(−7)	1.06(−3) − *i* 7.83(−7)	8.44(−4) − *i* 7.67(−7)
14	3.68(−3) − *i* 3.26(−5)	8.76(−4) − *i* 9.82(−7)	7.40(−4) − *i* 6.68(−5)	1.41(−3) − *i* 7.12(−5)	1.09(−3) − *i* 1.16(−7)	8.78(−4) − *i* 1.14(−7)
15	4.23(−3) − *i* 3.47(−4)	9.34(−4) − *i* 5.08(−5)	9.80(−4) − *i* 7.86(−7)	1.56(−3) − *i* 3.54(−4)	1.16(−3) − *i* 7.50(−5)	9.34(−4) − *i* 7.38(−5)
16	4.60(−3) − *i* 4.45(−5)	1.05(−3) − *i* 3.13(−4)	1.05(−3) − *i* 6.22(−7)	1.61(−3) − *i* 1.41(−5)	1.30(−3) − *i* 3.37(−4)	1.06(−3) − *i* 3.13(−4)
17		1.17(−3) − *i* 7.06(−7)	1.06(−3) − *i* 8.54(−7)	1.65(−3) − *i* 7.83(−4)	1.37(−3) − *i* 1.24(−5)	1.16(−3) − *i* 1.08(−5)
18		1.30(−3) − *i* 3.00(−4)	1.07(−3) − *i* 5.60(−6)	2.17(−3) − *i* 1.60(−5)	1.67(−3) − *i* 4.88(−5)	1.30(−3) − *i* 6.64(−7)
19		1.30(−3) − *i* 1.41(−6)	1.09(−3) − *i* 4.89(−7)	2.24(−3) − *i* 7.85(−4)	1.84(−3) − *i* 3.41(−4)	1.40(−3) − *i* 4.89(−5)
20		1.62(−3) − *i* 5.82(−7)	1.11(−3) − *i* 1.66(−6)		1.88(−3) − *i* 1.44(−5)	1.55(−3) − *i* 3.19(−4)
21		1.78(−3) − *i* 2.83(−4)	1.14(−3) − *i* 2.71(−5)		1.94(−3) − *i* 7.63(−4)	1.61(−3) − *i* 1.27(−5)
22					2.49(−3) − *i* 1.64(−5)	1.66(−3) − *i* 7.36(−4)
23					2.58(−3) − *i* 7.73(−4)	1.96(−3) − *i* 3.15(−5)
24						2.14(−3) − *i* 3.29(−4)
25						2.17(−3) − *i* 1.46(−5)
26						2.25(−3) − *i* 7.44(−4)
27						2.84(−3) − *i* 1.67(−5)
28						2.94(−3) − *i* 7.61(−4)

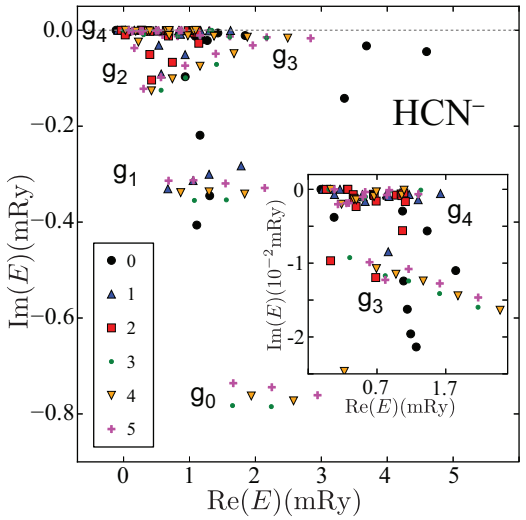

FIG. 4. (Color online) Predicted energies of the HCN^- dipolar anion for $J^\pi = 0^+, 1^-, 2^+, 3^-, 4^+$, and 5^- states in the complex-energy plane. Based on their complex energies, these states can be organized into five groups labeled g_0 to g_4. Bound states and near-threshold resonances belonging to g_4 and narrow resonances of g_3 are shown in the inset.

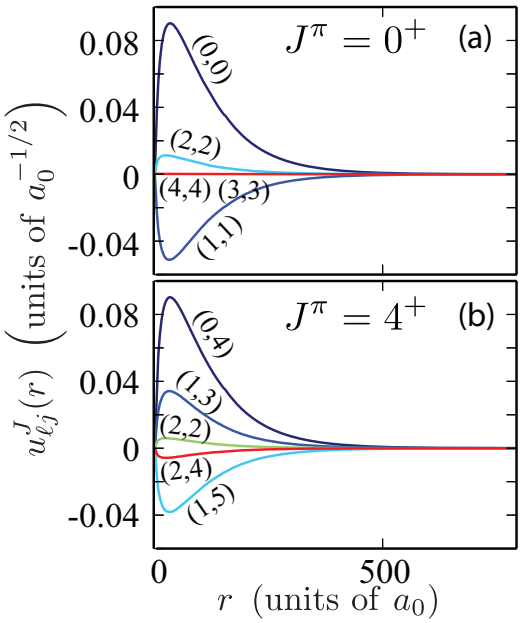

FIG. 6. (Color online) Channel wave functions (ℓ, j) of the (a) $J^\pi = 0_1^+$ and (b) 4_1^+ members of the ground-state rotational band in HCN^- in the adiabatic limit.

$(E = -1.2308 \times 10^{-4}$ Ry). We can conclude, therefore, that the members of the ground-state rotational band are practically degenerate in the adiabatic limit.

Figure 5 illustrates the intrinsic density for the ground-state band in the adiabatic limit ($I \to \infty; K_J = 0$). The intrinsic densities for all band members are numerically identical even though the associated wave functions in the laboratory system are different, see Fig. 6. The strongly asymmetric shape of electron's distribution reflects the attraction (or repulsion) between the electron and positive (or negative) charge of the dipole (for other illustrative examples, see Refs. [5,7,11,25,89]).

We found that the density representation given by Eq. (19) can also be useful in the nonadiabatic case, with finite moment of inertia, to assign members of rotational bands. This is illustrated in Fig. 7 which shows the density (19) for the bound states $J^\pi = 0_1^+, 1_1^-$, and 2_1^+ of HCN^-. Despite the fact that the strong coupling limit does not strictly apply in this case, distributions are practically identical and close to the intrinsic density displayed in Fig. 5.

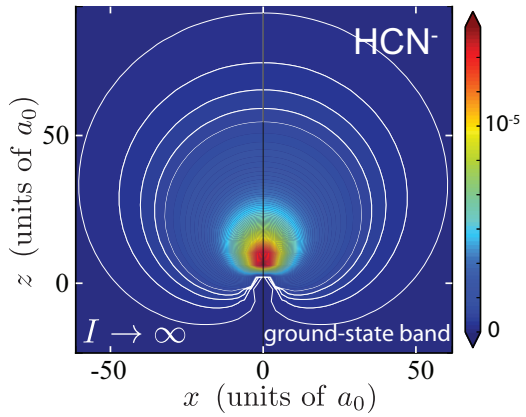

FIG. 5. (Color online) The intrinsic density of the valence electron in HCN^- in the ground-state rotational band $J^\pi = 0_1^+, 1_1^-, 2_1^+, 3_1^-, \ldots$. (All densities are in a_0^{-1}.)

B. Rotational bands

Excitation energies of the lowest-energy resonant (i.e., bound and resonance) states are plotted in Fig. 8 as a function of $J(J+1)$. The $J^\pi = 0^+, 1^-, 2^+$ bound states form a $K_J = 0$ rotational band as evidenced by their intrinsic densities shown in Fig. 7. Another $K_J = 0$ rotational band is built upon the 0_2^+ resonance. According to Table II, a 1_2^- member of this band has a decay width that is reduced by over three orders of magnitude as compared to that of the 0_2^+ band head. We predict other very narrow resonances as well. Among them, the 2_4^+ state has $K_J = 2$ while 1_4^- and 2_3^+ resonances have a mixed character.

As can be judged by results displayed in Fig. 8, except for few states with well-defined K_J values, the majority of resonances are strongly K_J mixed. Consequently, an identification of other rotational bands in the continuum, based on the concept of intrinsic density, is not straightforward. This is true, in particular for the supposed higher-J members of the ground-state band. Figure 9 shows $\rho_{JK_J=0}$ for $J^\pi = 3_1^-, 4_1^+, 5_1^-$ resonances, which are expected (based on energy considerations) to form a continuation of the ground-state rotational band. One can see that these densities are not only drastically different from those of $0_1^+, 1_1^-$, and 2_1^+ states, but also change from one state to another. It is also worth noting that the densities of $3_1^-, 4_1^+$, and 5_1^- resonances have spatial extensions that are dramatically larger as compared to the three bound members of the ground-state band.

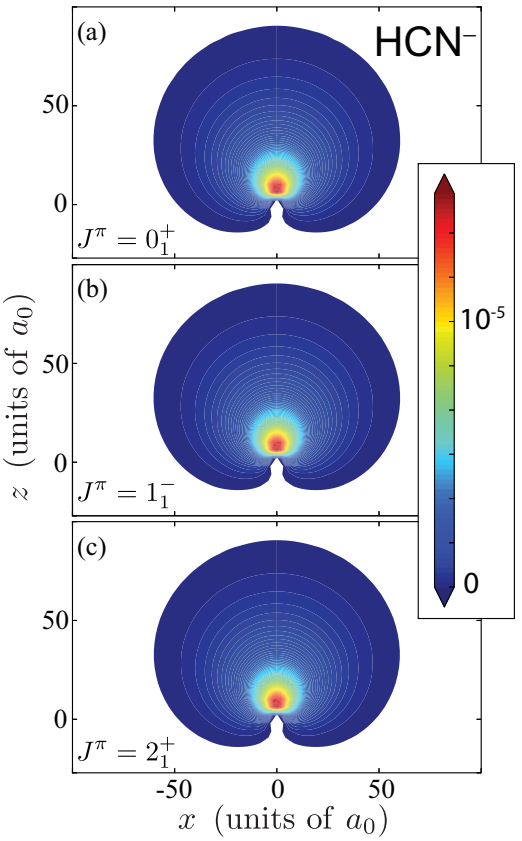

FIG. 7. (Color online) Density (19) of the valence electron in the bound states (a) $J^\pi = 0_1^+$, (b) 1_1^-, and (c) 2_1^+ of HCN^-. (All densities are in a_0^{-1}.)

As seen in Fig. 4, there appear clusters of resonances having the same total angular momentum J within one group g_i. In each cluster, the dominant channel wave functions have the same orbital angular momentum of the valence electron ℓ, but different rotational angular momenta of the molecule j. Excitation energies of resonances are plotted as a function of the molecular angular momentum j in Fig. 10 for different

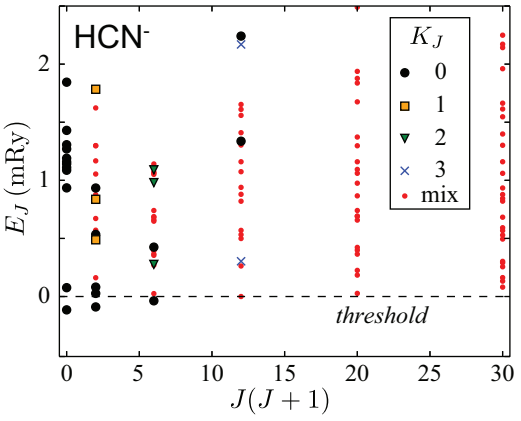

FIG. 8. (Color online) Energy spectrum of the HCN^- anion for $J^\pi = 0^+, 1^-, 2^+, 3^-, 4^+$, and 5^- shown as a function of $J(J+1)$. The dominant K_J component (21) is indicated. If several components are present, the state is marked as "mix."

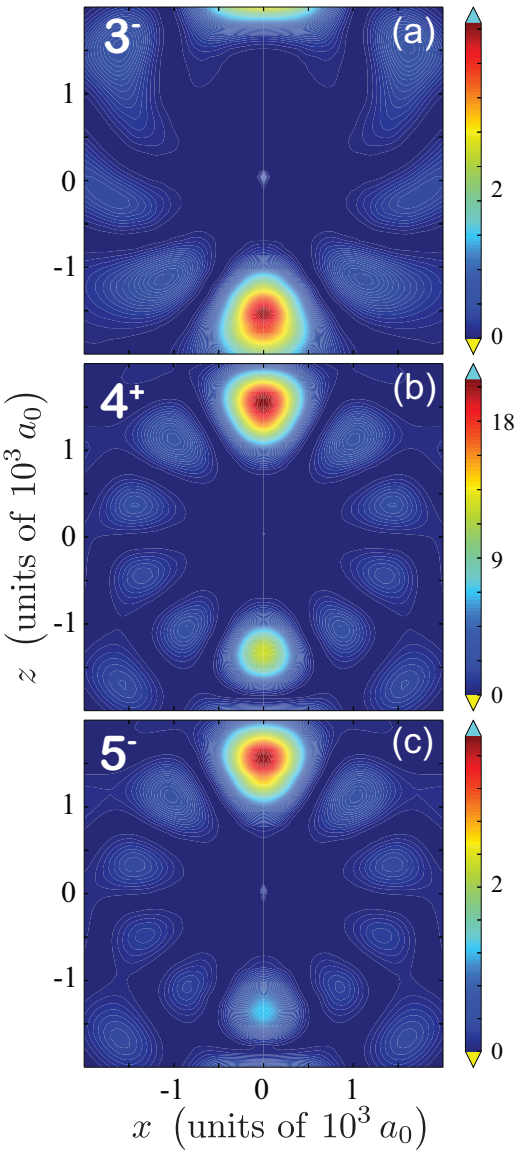

FIG. 9. (Color online) Similar as in Fig. 7 but for $\rho_{JK_J=0}(r,\theta)$ (in $10^{-15}\,a_0$) in (a) 3_1^-, (b) 4_1^+, and (c) 5_1^-.

groups of resonances of Fig. 4. It is seen that these states form very regular rotational band sequences in j rather than in J. Different members of such bands lie close in the complex energy plane and have similar densities $\rho_{JK_J}(r,\theta)$. This is illustrated in Fig. 11, which shows $\rho_{JK_J}(r,\theta)$ for the two $J^\pi = 5^-$ resonances marked by arrows in Fig. 10(c); namely 5_3^-, having the dominant parentage $(\ell, j) = (6,1)$, and 5_{23}^-, having the dominant parentage (6,11).

The results of Fig. 10 suggest that the rotational resonance structures are governed by a weak ℓ-j coupling, whereby the orbital motion of a valence electron is decoupled from the rotational motion of a dipolar neutral molecule. To illustrate the weak coupling better, in Fig. 12 we display the rotational bands of Fig. 10 with respect to the rigid rotor reference $j(j+1)/2I$. In the case of a perfect ℓ-j decoupling, the rescaled energy in Fig. 12 should be equal to 1. One can see that this limit is reached in most cases, with deviations from unity being less than 10%. Larger deviations are found

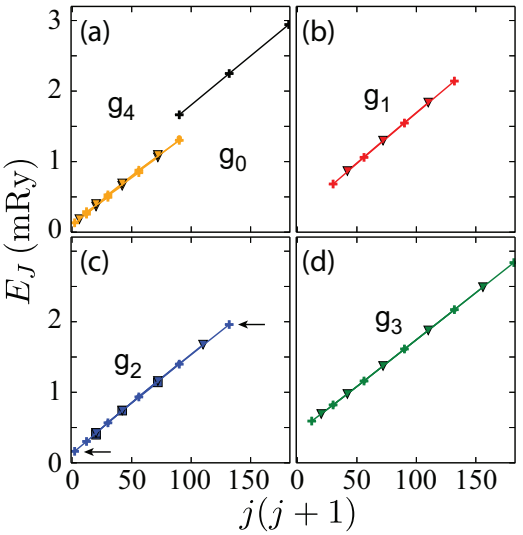

FIG. 10. (Color online) Excitation energies of resonances of the HCN^- dipolar anion for various J^π as a function of $j(j+1)$, where j is the rotational angular momentum of the molecule in the dominant channel wave function for each considered state. Colors are related to groups of states in the complex-energy plane identified in Fig. 4. The symbols ■, ●, ▼ and + denote states with $J^\pi = 2^+, 3^-, 4^+$, and 5^-, respectively.

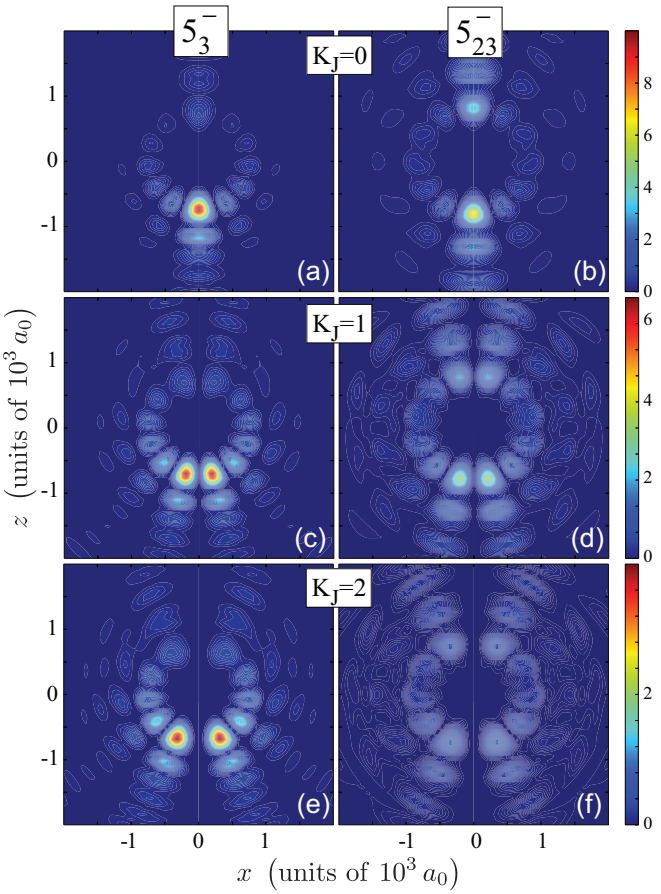

FIG. 11. (Color online) Intrinsic densities $\rho_{JK_J}(r,\theta)$ (in $10^{-10}\,a_0$) with $K_J = 0,1,2$, for the two resonances 5_3^- and 5_{23}^- belonging to the group g_2, marked by arrows in Fig. 10(c). For both states, the dominant channel has $\ell = 6$.

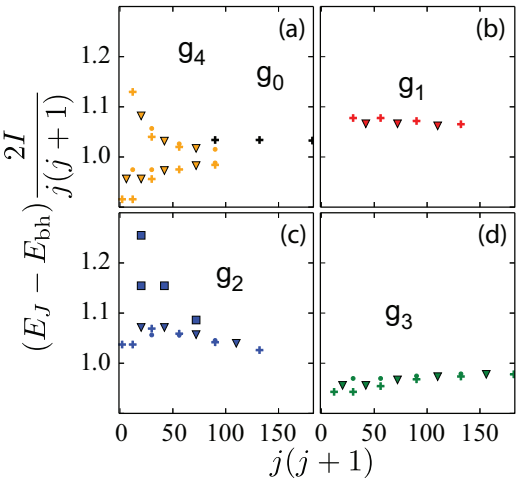

FIG. 12. (Color online) Similar as in Fig. 10 but for $(E_J - E_{bh})\frac{2I}{j(j+1)}$, where E_{bh} is a band-head energy at $j = 0$.

for few low-j states in bands with $J = 2$ in g_2 and $J = 5$ in g_4. Consequently, intrinsic densities for resonances in these two bands exhibit certain differences, whereas they are almost identical for bands close to the weak-coupling limit.

The variations seen in Fig. 12 can be traced back to the leading-channel components along a j band. Table III displays the leading channel wave functions to the resonances in different groups g_i. Not surprisingly, the resonances forming j-band structures are associated with high-orbital angular momentum components $\ell = 6$–9 for which the centrifugal force induces a strong decoupling of the electron and the rotor. For regular bands in Fig. 12, the ℓ content is almost constant as a function of j. For instance, for the four $J = 5$ states in g_1, the (ℓ, j) parentages of the two largest $(6,j)/(7,j+1)$ components are 0.64/0.37 ($j = 5$), 0.67/0.36 ($j = 7$), 0.69/0.35 ($j = 9$), and 0.70/0.34 ($j = 11$). On the other hand, for bands that exhibit stronger j dependence in Fig. 12 the ℓ compositions change.

Interesting complementary information about the arrangement of resonances in the continuum of HCN^- can be seen in Fig. 13 which shows the decay width for various j bands in different groups g_i and different total angular momenta J within a given group. One can see that the bands that exhibit largest deviations from the weak-coupling limit in Fig. 12, also show strong in-band variations of the decay width. In regular

TABLE III. Contributions of the two leading-channel wave functions to the norm of resonances in different groups of states in Fig. 4. Only states with dominant channel $\ell = 6$ for g_1, g_2, annd g_4, and $\ell = 8$ for g_0, and g_3 are included.

	ℓ of dominant channels			
Group	6	7	8	9
g_0	–	–	60%	40%
g_3	1%	–	99%	–
g_1	70%	30%	–	–
g_2	90%	10%	–	–
g_4	100%	–	–	–

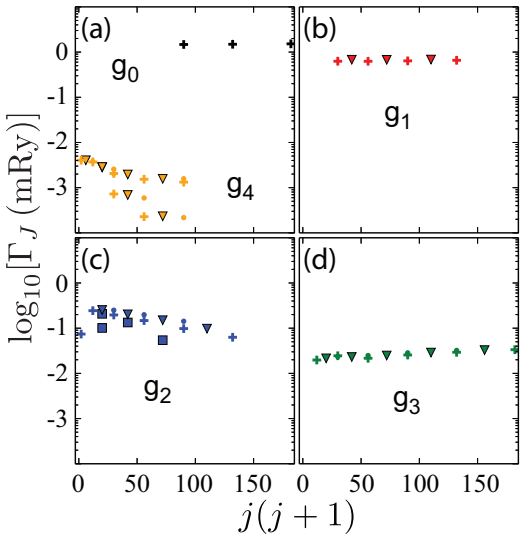

FIG. 13. (Color online) Similar as in Fig. 10 but for the resonance widths.

bands belonging to g_0, g_1, and g_3, the width stays constant or slightly increases with j. On the other hand, the irregular bands in g_2 and g_4 exhibit a decrease of Γ_J with j. Such a behavior of lifetimes can be traced back to variations of the (ℓ, j) content of the resonance wave function with rotation.

IX. CONCLUSION

In this work, we studied bound and resonance states of the dipole-bound anion of hydrogen cyanide HCN^- using an open-system quantum-mechanical approach: the Berggren expansion method. To identify the decaying resonant states and separate them from the scattering background, we adopted the algorithm based on contour shift in the complex energy plane. To characterize spatial distributions of valence electrons, we introduced the intrinsic density of the valence electron. This quantity is useful when assigning resonant states into rotational bands.

Dipole molecules contain large numbers of electrons and this makes *ab initio* treatments difficult. However, since we are interested in a description of a near-threshold spectrum of an anion rather than the whole molecular spectrum, we use a phenomenological approach based on a pseudopotential, with few parameters adjusted to experiment. This guarantees that all important reaction thresholds are described correctly, and this is essential for the description of one-electron continuum. The use of a pseudopotential is well justified by a scale separation between the slow s.p. motion of the attached electron (comparable to rotational excitations of the molecule) and fast s.p. motion of HCN electrons. Such a mismatch of scales, well known in the field of quantum halos, guarantees the validity of an effective interaction treatment [68–70]. The low ionization energy implies that the familiar Born-Oppenheimer approximation breaks down so the motion of the valence electron is highly nonadiabatic.

Since the pseudopotential used is non-dilatation-analytic, it cannot be treated by a complex-coordinate method. Hence, available methods to treat this type of problems reduce to two classes of models. The first class of models can be associated with CESE [63,64], where the Hamiltonian coordinates are not complex-rotated and its eigenfunctions are split in two parts, an inner localized part and an outer part of outgoing character. Exterior complex scaling can thus be applied to the wave function to make it normalizable. The second class of models concerns BEM, where Hamiltonian coordinates remain real and the exterior complex scaling is utilized, but which is based on a diagonalization procedure using nonlocalized basis; this implies that the asymptotic form of eigenfunctions is not predefined and comes naturally from the configuration mixing. While both methods are theoretically equivalent, the imposition of the outgoing asymptotics would be difficult in the studied case of the HCN^- anion. Indeed, due to the slowly decaying dipole potential, the exponential asymptotic is attained only at distances of tens of thousands of a_0.

Nonadiabatic coupled-channel calculations with a pseudopotential adjusted to ground-state properties of HCN^- predict only three bound states of the dipole-bound anion: $0^+, 1^-$, and 2^+. Those states are members of the ground-state rotational band. The lowest 3^-_1 state is a threshold resonance; its intrinsic structure is very different from that of $0^+_1, 1^-_1$, and 2^+_1 states, and the lowest-energy resonances 4^+_1 and 5^-_1.

The dissociation threshold in the HCN^- dipolar anion defines two distinct regimes of rotational motion. Below the threshold, rotational bands in J can be associated with bound states. Here, the valence electron follows the collective rotation of the molecule. This is not the case above the threshold where the motion of a valence electron in a resonance state is largely decoupled from the molecular rotation with the families of resonances forming regular band sequences in j. Widths of resonances forming j bands depend primarily on the electron's orbital angular momentum in the dominant channel and remain fairly constant within each band for regular bands. Small irregularities in moments of inertia and decay width are predicted for very narrow resonances in the vicinity of the dissociation threshold.

In summary, this work demonstrates the feasibility of accurate calculations of weakly bound and unbound states of the dipolar anions using a nonadiabatic pseudopotential method and the Berggren expansion approach. Our prediction of two distinct modes of rotation in this open quantum system awaits experimental confirmation. It is interesting to note a similarity between the problem of a dipolar anion and a coupling of electrons in high molecular Rydberg states to molecular rotations [90,91]. Namely, in both cases one deals with the nonadiabatic coupling of a slow electron to the fast rotational motion of the core, with no separation in the single-particle and collective time scales.

ACKNOWLEDGMENTS

Discussions with R. N. Compton and W. R. Garrett are gratefully acknowledged. This material is based upon work supported by the U.S. Department of Energy, Office of Science, Office of Nuclear Physics under Award No. DEFG02-96ER40963 (University of Tennessee). This work was supported partially through FUSTIPEN (French-U.S. Theory Institute for Physics with Exotic Nuclei) under DOE Grant No. DE-FG02-10ER41700.

[1] W. R. Garrett, Chem. Phys. Lett. **5**, 393 (1970); Phys. Rev. A **3**, 961 (1971).
[2] S. F. Wong and G. J. Schulz, Phys. Rev. Lett. **33**, 134 (1974).
[3] K. D. Jordan, J. Chem. Phys. **66**, 3305 (1977).
[4] K. D. Jordan and F. Wang, Annu. Rev. Phys. Chem. **54**, 367 (2003).
[5] C. Desfrançois, H. Abdoul-Carime, and J. P. Schermann, Int. J. Mol. Phys. B **10**, 1339 (1996); H. Abdoul-Carime and C. Desfrançois, Eur. Phys. J. D **2**, 149 (1998).
[6] R. N. Compton and N. I. Hammer, *Advances in Gas Phase Ion Chemistry*, Vol. 4 (Elsevier, New York, 2001).
[7] C. Desfrançois, Y. Bouteiller, J. P. Schermann, D. Radisic, S. T. Stokes, K. H. Bowen, N. I. Hammer, and R. N. Compton, Phys. Rev. Lett. **92**, 083003 (2004).
[8] L. Adamowicz and R. J. Bartlett, J. Chem. Phys. **83**, 6268 (1985).
[9] G. L. Gutsev, M. Nooijen, and R. J. Bartlett, Chem. Phys. Lett. **276**, 13 (1997).
[10] G. L. Gutsev, M. Nooijen, and R. J. Bartlett, Phys. Rev. A **57**, 1646 (1998).
[11] J. Simons, J. Phys. Chem. **112**, 6401 (2008).
[12] E. Fermi and E. Teller, Phys. Rev. **72**, 399 (1947).
[13] J.-M. Lévy-Leblond, Phys. Rev. **153**, 1 (1967).
[14] K. Riisager, D. V. Fedorov, and A. S. Jensen, Europhys. Lett. **49**, 547 (2000).
[15] A. S. Jensen, K. Riisager, D. V. Fedorov, and E. Garrido, Rev. Mod. Phys. **76**, 215 (2004).
[16] J. Mitroy, Phys. Rev. Lett. **94**, 033402 (2005).
[17] S. Knoop, F. Ferlaino, M. Mark, M. Berninger, H. Schobel, H. C. Nagerl, and R. Grimm, Nat. Phys. **5**, 227 (2009).
[18] H.-W. Hammer and L. Platter, Ann. Rev. Nucl. Part. Sci. **60**, 207 (2010).
[19] F. Ferlaino and R. Grimm, Physics **3**, 9 (2010).
[20] K. R. Lykke, R. D. Mead, and W. C. Lineberger, Phys. Rev. Lett. **52**, 2221 (1984).
[21] J. Marks, D. M. Wetzel, P. B. Comita, and J. I. Brauman, J. Chem. Phys. **84**, 5284 (1986).
[22] T. Andersen, Phys. Scr. **1991**, 23 (1991).
[23] E. A. Brinkman, S. Berger, J. Marks, and J. I. Brauman, J. Chem. Phys. **99**, 7586 (1993).
[24] A. S. Mullin, K. K. Murray, C. P. Schulz, and W. C. Lineberger, J. Phys. Chem. **97**, 10281 (1993).
[25] S. Ard, W. R. Garrett, R. N. Compton, L. Adamowicz, and S. G. Stepanian, Chem. Phys. Lett. **473**, 223 (2009).
[26] T. F. O'Malley, Phys. Rev. **137**, A1668 (1965).
[27] H. Estrada and W. Domcke, J. Phys. B : At. Mol. Phys. **17**, 279 (1984).
[28] C. W. Clark, Phys. Rev. A **30**, 750 (1984).
[29] I. I. Fabrikant, J. Phys. B **18**, 1873 (1985).
[30] D. C. Clary, J. Phys. Chem. **92**, 3173 (1988).
[31] D. C. Clary, Phys. Rev. A **40**, 4392 (1989).
[32] M. McCartney, P. G. Burke, L. A. Morgan, and C. J. Gillan, J. Phys. B **23**, L415 (1990).
[33] H. R. Sadeghpour, J. L. Bohn, M. J. Cavagnero, B. D. Esry, I. I. Fabrikant, J. H. Macek, and A. R. P. Rau, J. Phys. B **33**, R93 (2000).
[34] J. Martorell, J. G. Muga, and D. W. L. Sprung, Phys. Rev. A **77**, 042719 (2008).
[35] W. R. Garrett, J. Chem. Phys. **77**, 3666 (1982).
[36] W. R. Garrett, J. Chem. Phys. **133**, 224103 (2010).
[37] H. E. Camblong, L. N. Epele, H. Fanchiotti, and C. A. García Canal, Phys. Rev. Lett. **87**, 220402 (2001).
[38] S. A. Coon and B. R. Holstein, Am. J. Phys. **70**, 513 (2002); M. Bawin and S. A. Coon, Phys. Rev. A **67**, 042712 (2003); M. Bawin, S. A. Coon, and B. R. Holstein, Int. J. Mod. Phys. A **22**, 4901 (2007).
[39] K. Fossez, N. Michel, W. Nazarewicz, and M. Płoszajczak, Phys. Rev. A **87**, 042515 (2013).
[40] T. Berggren, Nucl. Phys. A **389**, 261 (1982).
[41] T. Berggren and P. Lind, Phys. Rev. C **47**, 768 (1993).
[42] P. Lind, Phys. Rev. C **47**, 1903 (1993).
[43] T. Berggren, Nucl. Phys. A **109**, 265 (1968).
[44] L. S. Ferreira, E. Maglione, and R. J. Liotta, Phys. Rev. Lett. **78**, 1640 (1997).
[45] A. T. Kruppa, B. Barmore, W. Nazarewicz, and T. Vertse, Phys. Rev. Lett. **84**, 4549 (2000).
[46] B. Barmore, A. T. Kruppa, W. Nazarewicz, and T. Vertse, Phys. Rev. C **62**, 054315 (2000).
[47] A. T. Kruppa and W. Nazarewicz, Phys. Rev. C **69**, 054311 (2004).
[48] Y. Jaganathen, N. Michel, and M. Płoszajczak, J. Phys.: Conf. Ser. **403**, 012022 (2012); Phys. Rev. C **89**, 034624 (2014).
[49] R. I. Betan, A. T. Kruppa, and T. Vertse, Phys. Rev. C **78**, 044308 (2008); R. I. Betan, Phys. Lett. B **730**, 18 (2014).
[50] V. E. Chernov, A. V. Dolgikh, and B. A. Zon, Phys. Rev. A **72**, 052701 (2005).
[51] J. N. Bardsley, Int. J. Q. Chem. **14**, 343 (1978).
[52] C. A. Nicolaides and D. R. Beck, Int. J. Quant. Chem. **14**, 457 (1978).
[53] B. Simon, Phys. Lett. A **71**, 211 (1979).
[54] Y. Ho, Phys. Rep. **99**, 1 (1983).
[55] Y. K. Ho, Phys. Rev. A **45**, 148 (1992).
[56] N. Moiseyev, Phys. Rep. **302**, 212 (1998).
[57] M. Bylicki and C. A. Nicolaides, Phys. Rev. A **61**, 052508 (2000).
[58] B. Junker, *Recent Computational Developments in the use of Complex Scaling in Resonance Phenomena* (Academic, New York, 1982), pp. 207–263.
[59] A. T. Kruppa, G. Papadimitriou, W. Nazarewicz, and N. Michel, Phys. Rev. C **89**, 014330 (2014).
[60] H. Masui, K. Katō, N. Michel, and M. Płoszajczak, Phys. Rev. C **89**, 044317 (2014).
[61] J. Aguilar and J. M. Combes, Commun. Math. Phys. **22**, 269 (1971).
[62] E. Balslev and J. M. Combes, Commun. Math. Phys. **22**, 280 (1971).
[63] C. A. Nicolaides and S. I. Themelis, Phys. Rev. A **45**, 349 (1992).
[64] C. A. Nicolaides, Adv. Quantum Chem. **60**, 163 (2010).
[65] T. Klahn and P. Krebs, J. Chem. Phys. **109**, 531 (1998).
[66] P. Skurski, M. Gutowski, and J. Simons, J. Chem. Phys. **114**, 7443 (2001).
[67] K. A. Peterson and M. Gutowski, J. Chem. Phys. **116**, 3297 (2002).
[68] C. Bertulani, H.-W. Hammer, and U. van Kolck, Nucl. Phys. A **712**, 37 (2002).
[69] P. Bedaque, H.-W. Hammer, and U. van Kolck, Phys. Lett. B **569**, 159 (2003).
[70] G. Rupak and R. Higa, Phys. Rev. Lett. **106**, 222501 (2011).

[71] W. R. Garrett, J. Chem. Phys. **71**, 651 (1979).
[72] W. R. Garrett, J. Chem. Phys. **73**, 5721 (1980).
[73] W. R. Garrett, Phys. Rev. A **22**, 1769 (1980).
[74] W. R. Garrett, Phys. Rev. A **23**, 1737 (1981).
[75] N. Michel, W. Nazarewicz, M. Płoszajczak, and T. Vertse, J. Phys. G **36**, 013101 (2009).
[76] B. Gyarmati and T. Vertse, Nucl. Phys. A **160**, 523 (1971).
[77] A. Nicolaides and D. R. Beck, Phys. Lett. A **65**, 11 (1978).
[78] C. A. Nicolaides, H. J. Gotsis, M. Chrysos, and Y. Komninos, Chem. Phys. Lett. **168**, 570 (1990).
[79] A. M. Dykhne and A. V. Chaplik, Sov. Phys. JETP **13**, 1002 (1961).
[80] N. Michel, W. Nazarewicz, M. Płoszajczak, and K. Bennaceur, Phys. Rev. Lett. **89**, 042502 (2002).
[81] N. Michel, W. Nazarewicz, M. Płoszajczak, and J. Okołowicz, Phys. Rev. C **67**, 054311 (2003).
[82] J. H. Van Vleck, Rev. Mod. Phys. **23**, 213 (1951).
[83] G. Herzberg, *Molecular Spectra and Structure. III. Electronic Spectra and Electronic Structure of Polyatomic Molecules* (Van Nostrand and Reinhold, New York, 1966).
[84] A. Bohr and B. R. Mottelson, *Nuclear Structure, Vol. 2: Nuclear Deformations* (World Scientific, Singapore, 1998).
[85] A. T. Kruppa, W. Nazarewicz, and P. B. Semmes, AIP Conf. Proc. **518**, 173 (2000).
[86] A. T. Kruppa and W. Nazarewicz, AIP Conf. Proc. **681**, 61 (2003).
[87] H. Esbensen and C. N. Davids, Phys. Rev. C **63**, 014315 (2000).
[88] C. N. Davids and H. Esbensen, Phys. Rev. C **69**, 034314 (2004).
[89] P. D. Burrow, G. A. Gallup, A. M. Scheer, S. Denifl, S. Ptasinska, T. Märk, and P. Scheier, J. Chem. Phys. **124**, 124310 (2006).
[90] J. Dagata, L. Klasinc, and S. McGlynn, Pure Appl. Chem. **61**, 2151 (1989).
[91] F. Remacle and R. D. Levine, J. Chem. Phys. **104**, 1399 (1996).